Spin-polarized field emission from Ni(001) and Ni(111) surfaces

T. Ohwaki,[1] D. Wortmann,[2] H. Ishida,[3] S. Blügel,[2] and K. Terakura[1,4]
[1]*Research Institute for Computational Sciences, AIST, Tsukuba, Ibaraki 306-8568, Japan*
[2]*Institut für Festkörperforschung, Forschungszentrum Jülich, 52425 Jülich, Germany*
[3]*CREST, JST, and Nihon University, Sakura-josui, Tokyo 156-8550, Japan*
[4]*Creative Research Initiative "Sousei," Hokkaido University, N21W10 Kita-ku, Sapporo 001-0021, Japan*
(Received 29 March 2006; published 22 June 2006)

Results are presented of a first-principles calculation of the spin-polarized field emission from ferromagnetic Ni(111) and Ni(001) surfaces. The electronic structure of both surfaces exposed to an external field is determined by combining the surface-embedded Green function approach and the full-potential linearized augmented plane-wave (FLAPW) method within the local spin density approximation. We discuss the contributions of different states to the field-emission current. In particular, we show that delocalized states make similar contributions to that obtained at jellium surfaces while localized Ni *d* states contribute mostly through surface states and resonances. These contributions dominate in the minority spin and lead to a negative spin polarization of the emitted current.

DOI: 10.1103/PhysRevB.73.235424 PACS number(s): 73.20.At, 79.70.+q, 72.25.Mk, 71.15.Mb

I. INTRODUCTION

Spin-polarized electron tunneling is a subject of great current interest. In particular, the rapid progress in the fabrication of nanoscale magnetic tunnel-junctions[1,2] and their application in magnetoelectronic and spintronic devices as well as the development of the spin-polarized scanning tunneling microscopy (SP-STM)[3] revitalized the field which was already studied in the last century.

While the basic phenomena of electron tunneling are well-understood, the quantitative theoretical description of the spin polarization in the tunneling current is extremely difficult for real systems. The spin polarization is a result of a subtle cancellation between two spin channels and is greatly affected by the details of atomic, electronic, and magnetic structures of the system. Such information is generally lacking at the interfaces of actual tunnel-junctions. The situation is not much improved even for STM since the details of the tip-geometry can only be speculated about. Therefore, one frequently works with simplified theoretical models, such as Julliere's model[4] for magnetic tunnel-junctions or the model for SP-STM proposed by Wortmann *et al.*[5] Common to these models is the proportionality of the spin-polarized current to the convolution of the spin-resolved density of states (DOS) in the vicinity of the Fermi level of the two leads.

On the other hand, field emission from a planar surface has a distinct advantage of using a well-defined surface as an interface. Thus spin-resolved field emission offers an excellent opportunity to investigate the detailed mechanism of the spin-polarization in the tunneling current.

Theory of field emission dates back to the pioneering work of Fowler and Nordheim.[6] Subsequent studies were based on one-dimensional model potentials,[7] the layer-Korringa-Kohn-Rostoker (LKKR) method,[8–10] and jellium-electrode models.[11–14] Recently, two of the authors and Liebsch presented a first-principles method for the evaluation of field-emission currents from semi-infinite crystal surfaces. The method was applied for the calculation of field emission from noble metal surfaces[15] and stepped Pd and Pt surfaces.[16] The virtue of such a half-space geometry is that bulk states form continuous energy spectra so that the discrete level spacing inherent in conventional repeated slab calculations can be avoided. This is particularly important for an accurate treatment of electron emission which is essentially limited to a range of a few tenths of an eV below the Fermi level E_F.

In the present paper, we apply the above-mentioned calculational scheme to the field emission from ferromagnetic Ni(001) and (111) surfaces. Ni surfaces are strong ferromagnets with a large difference in the density of states at the Fermi level between majority and minority spin electrons, such that large effects can be expected. In the past, several experimental[17–20] and theoretical studies[21–24] were conducted on the spin polarization of field-emitted electrons from Ni surfaces, aiming at obtaining the basic knowledge of the electronic structure of ferromagnetic Ni surfaces. For Ni(001), Modinos and Oxinos[23] conducted a field-emission calculation based on an LKKR approach within spherical muffin-tin (MT) potentials, empirical surface potential barriers, and the Wenzel-Kramers-Brillouin (WKB) approximation for the tunneling probability. They found that the *sp* bands contribute most of the field-emission current. The calculated spin polarization P varied between -0.99% to -11.198% depending on the potential form (the minus sign signifies a larger current due to minority-spin electrons). A similar calculation was performed by Zavadil and Modinos[24] for Ni(111). The calculated P varied largely and even changed sign depending on the bulk and surface potentials chosen. The main reason of such subtleties in the spin-polarization of the emission current is that the *d* states being responsible to the dominant contribution to the DOS near the Fermi level are fairly localized in space and that they do not necessarily make dominant contributions to the emission current. In order to make the situation clearer, we perform field-emission calculations where the surface potential is determined self-consistently. Such calculations for the Ni(001) and Ni(111) surfaces have not been available to date. The most important result in the present study is that the calcu-

lated P is definitely negative for both Ni(001) and Ni(111). The origin of negative P will be discussed in detail.

The outline of the present paper is as follows. In Sec. II we briefly explain the method for calculating the self-consistent surface electronic structure and the tunneling current. Section III is the main part of the present paper and contains calculated results and discussion. Finally, a summary is given in Sec. V. We use the Hartree atomic units throughout the paper unless otherwise stated.

II. METHOD

We calculate the electronic structure of a semi-infinite surface exposed to an external electric field within the local spin density approximation (LSDA), using the embedded Green-function technique of Inglesfield[25] and the full-potential linearized augmented plane wave (FLAPW) method.[15,26] The calculation proceeds in three steps: (i) the calculation of the bulk crystal potential using a bulk electronic-structure code, (ii) the construction of the embedding potential of a semi-infinite substrate for a given crystal orientation from the complex band structure,[27] and (iii) a self-consistent Green-function calculation in the embedded surface region. The bulk calculation was carried out at the experimental lattice constant (3.52 Å) and the surface relaxation was not taken into account in the surface calculation (see the comments in the next section). We incorporated the two outermost atomic layers in the embedded surface region.[28] The plane-wave cutoff for the Green-function expansion was chosen as 16 Ry. We used 18×18 $\mathbf{k}_\parallel$ mesh points in the surface Brillouin zone (SBZ) to determine self-consistent charge densities and potentials, where $\mathbf{k}_\parallel$ is a two-dimensional (2D) wave vector. For evaluating the field-emission current, we adopted 200×200 or 400×400 $\mathbf{k}_\parallel$ mesh points and 100 energy-mesh points in the energy window with a width of 1.5 eV below E_F. The Cartesian coordinates of our calculation systems are defined for each surface: (x, y, z) for the (001) surface and (x', y', z') for the (111) surface.[29] The z and z' axes are along the surface normal on each surface.

The field-emission current into the vacuum induced by an electric field consists of two components. There is the contribution of bulk states, which can be described by coherent single particle states and is easily computed by using the Landauer formula.[30,31] Additionally there can be a contribution to the field-emission current from electronic tunneling out of localized surface states. This contribution involves scattering processes coupling the surface state to the bulk states of the semi-infinite crystal such as electron-electron scattering, electron-phonon scattering, or scattering of the single particle states due to the presence of crystal imperfections. These processes are not included in our description of the system in the DFT scheme. However, assuming that the tunneling process itself is the rate-limiting process one can calculate the contribution of this noncoherent field-emission current by a perturbative ansatz within the single-particle DFT picture.

Both contributions to the field-emission current can easily be calculated within the framework of the embedded Green function method. The Landauer formula giving the coherent current can be expressed as a surface integral over a two-dimensional surface S normal to the direction of the current separating the left half-space containing the semi-infinite bulk from the vacuum in the right half-space.[27,32,33]

$$\Gamma_{\mathrm{L}}(\epsilon) = 2\int_S \rho_L(\mathbf{x},\mathbf{x}',\epsilon)\,\mathrm{Im}\,\Sigma_R(\mathbf{x}',\mathbf{x},\epsilon)\,d\mathbf{x}\,d\mathbf{x}' = 2\,\mathrm{Tr}[\rho_L\,\mathrm{Im}\,\Sigma_R], \tag{1}$$

where ϵ is the one-electron energy, Σ_R is the embedding potential for the right half-space, and ρ_L denotes the left spectral function. The incoherent contribution due to possible surface states can be approximated by[32]

$$\Gamma_{\mathrm{ss}}(\epsilon) = 2\,\mathrm{Tr}[\rho_R\,\mathrm{Im}\,\Sigma_R]. \tag{2}$$

Summing up Eqs. (1) and (2), one obtains the total tunneling conductance,

$$\Gamma(\epsilon) = 2\,\mathrm{Tr}[\rho\,\mathrm{Im}\,\Sigma_R], \tag{3}$$

where $\rho=\rho_L+\rho_R$, the total spectral function, can be expressed as the imaginary part of the retarded Green function. As discussed in Ref. 32 it is only permissible to add the surface state contribution to the Landauer result of Eq. (1) for sufficiently large barriers in which the separating surface S is placed sufficiently close to the surface side of the vacuum barrier. When calculating the contribution of the surface states one encounters a sharply peaked contribution which for a typical field strength in field-emission experiments has a width only of the order of 10^{-4}–10^{-7} eV. Thus one would need a very dense energy mesh to integrate the resonant peak correctly. To avoid this difficulty, we replace the spectral function in Eq. (3) by

$$\tilde{\rho}(\mathbf{x},\mathbf{x}',\epsilon) = -\frac{1}{\pi}\,\mathrm{Im}\,G(\mathbf{x},\mathbf{x}',\epsilon+i\eta), \tag{4}$$

where we have introduced an artificial broadening parameter η in the Green function, which is justified as far as $\mathrm{Im}\,\Sigma_R$ in Eq. (3) varies very little on the energy scale of η. For more details, see the original derivation in Ref. 32.

For a system which is periodic in the surface plane, the tunneling conductance becomes diagonal with respect to $\mathbf{k}_\parallel$, which enables us to define the $\mathbf{k}_\parallel$-resolved tunneling conductance $\Gamma(\epsilon,\mathbf{k}_\parallel)$ by

$$\Gamma(\epsilon) = \int_{\mathrm{SBZ}} \frac{d\mathbf{k}_\parallel}{(2\pi)^2}\Gamma(\epsilon,\mathbf{k}_\parallel), \tag{5}$$

where SBZ denotes the surface Brillouin zone. We also define the $\mathbf{k}_\parallel$-resolved current density by

$$J(\mathbf{k}_\parallel) = \int^{E_F} d\epsilon\,\Gamma(\epsilon,\mathbf{k}_\parallel). \tag{6}$$

The current density J for each spin is obtained either by integrating $\Gamma(\epsilon)$ up to E_F or by integrating $J(\mathbf{k}_\parallel)$ over the SBZ.

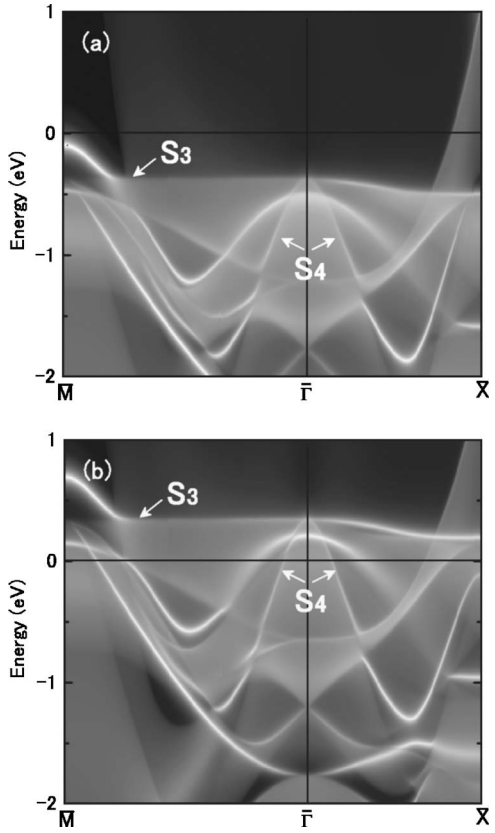

FIG. 1. Intensity plot of the $\mathbf{k}_{\parallel}$-resolved DOS calculated in a first-layer Ni MT sphere for a field-free Ni(001) surface. (a) Majority spin and (b) minority spin.

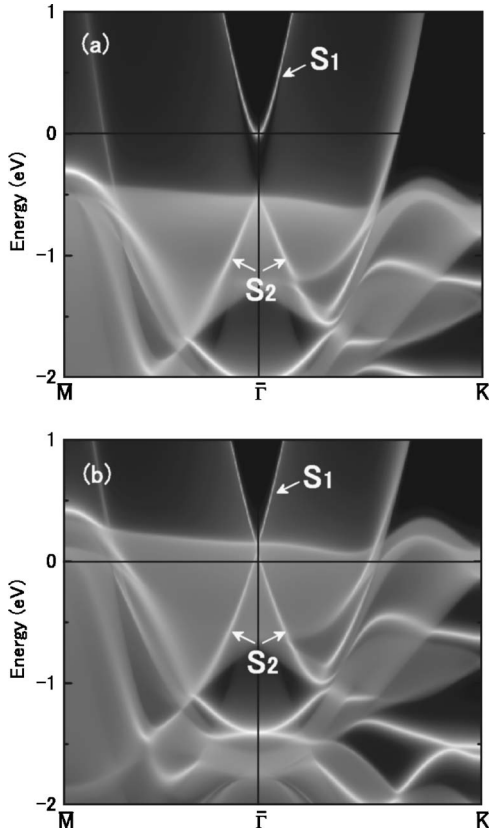

FIG. 2. Intensity plot of the $\mathbf{k}_{\parallel}$-resolved DOS calculated in a first-layer Ni MT sphere for a field-free Ni(111) surface. (a) Majority spin and (b) minority spin.

III. RESULTS AND DISCUSSION

A. Electronic structures of Ni surfaces

A number of first-principles calculations based on slab models were reported on the electronic and magnetic properties of Ni surfaces.[34–41] The change in the first interlayer spacing, Δ_{12}, was also investigated both experimentally[42,43] and computationally,[39] and was found to be a few percent. In our calculations, the surface relaxations change work functions and magnetic moments only of the order of 0.1% and the spin-polarization of tunneling conductance by less than a few percent. Hence we will show hereafter calculated results for unrelaxed Ni surfaces.

The calculated work functions for the Ni(111) and Ni(001) surfaces, 5.46 and 5.31 eV, are in good agreement with the experimental values (5.35 and 5.22 eV for the two surfaces, respectively[44]). This is crucial, since the work function determines the barrier height for electron tunneling.

Field-emission currents depend sensitively both on the projected band structure of a bulk metal and on localized surface states. In Fig. 1 we show an intensity plot in the $\mathbf{k}_{\parallel} - \epsilon$ plane of the $\mathbf{k}_{\parallel}$-resolved density of states (DOS) calculated in a top-layer Ni MT sphere for the Ni(001) surface, where the origin of energy is chosen as E_F.[45] The bright and dark colors correspond to large and small values of the DOS, respectively. The white thick lines indicate energy dispersions of either localized surface states, surface resonances, or the edges of projected bulk bands with a singular DOS. In Fig. 1, we especially pay attention to two Ni-3d surface-induced states denoted by S_3 and S_4. S_3 traverses the SBZ with a rather small energy dispersion as a resonance state and becomes a localized surface state in the energy gap near $\bar{M}$. The surface resonance state labeled by S_4 in Fig. 1 has a similar energy as S_3 near $\bar{\Gamma}$ but shows a strong downward dispersion. In the majority spin, S_3 and S_4 are separated from E_F by more than several tenths of eV toward lower energies. For the minority spin, it is seen that S_4 crosses E_F near $\bar{\Gamma}$.

In Fig. 2 we show the $\mathbf{k}_{\parallel}$-resolved DOS calculated in a top-layer MT sphere for the Ni(111) surface. The dark parabolic area having its minimum at $\bar{\Gamma}$ is an energy gap of the Ni bulk bands projected onto the SBZ. At $\bar{\Gamma}$, this gap corresponds to the $L_{2'}$-L_1 gap at the L point of the bulk BZ. Along the boundary between this energy gap and the projected bulk states, one can see a surface-induced state denoted by S_1. S_1 of the majority spin is a Shockley surface state in the energy gap. Its minimum at $\bar{\Gamma}$ is located below E_F by 0.005 eV.[46] This is consistent with photoemission measurements indicating that the minimum of S_1 is below E_F.[47,48] In contrast, S_1 of the minority spin merges into the projected Ni 3d bulk band at small $\mathbf{k}_{\parallel}$. In this $\mathbf{k}_{\parallel}$ range, S_1 turns into a resonance. At the same time, its spectral weight diminishes rapidly with decreasing $\mathbf{k}_{\parallel}$, until the peak in DOS vanishes at $\bar{\Gamma}$. The dispersion of S_1 of the minority spin deviates largely from a qua-

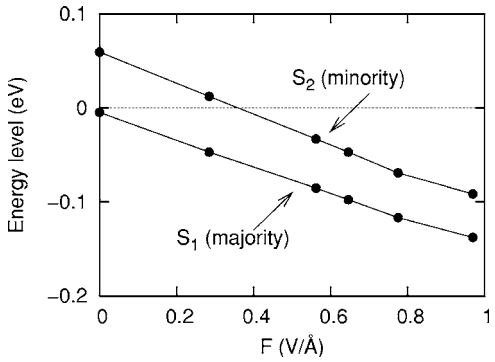

FIG. 3. Energy shifts of two surface states on the Ni(111) surface at $\bar{\Gamma}$ as a function of field strength.

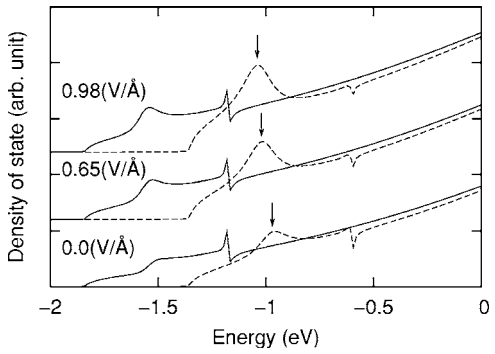

FIG. 4. The p_z component of the $\mathbf{k}_\parallel$-resolved DOS calculated in a top-layer Ni MT sphere for Ni(001) at $\bar{\Gamma}$. $F=0.0$, 0.65, and 0.98 V/Å from the bottom to the top. Solid and dashed lines correspond to the majority and minority spins, respectively.

dratic form. A second state with a large weight at the surface is labeled by S_2. In the majority spin it exhibits a downward dispersion in the energy range between −0.5 and −2.0 eV relative to E_F. The associated DOS peak becomes weaker with decreasing $\mathbf{k}_\parallel$ until it vanishes at $\bar{\Gamma}$. In contrast, S_2 of the minority spin has a large spectral weight at $\bar{\Gamma}$. In the Appendix, we summarize further details about the character of above-mentioned states, S_{1-4}, in terms of orbital components.

B. Field effects on surface electronic structures

The field strength F in typical field-emission experiments using a needle-shaped electrode is less than ~0.5 V/Å. For nanoscale electrodes it may be possible to achieve larger F values. Thus, in the present study, we extend calculations up to $F\sim 1$ V/Å. These electric fields will modify the surface electronic structure. Especially, localized surface states which have large amplitude even in the vacuum region, for example, S_1 and S_2 of the (111) surface, are sensitive to an applied field.[15] [Note, however, that the field-induced shift of resonance states with a large d-orbital component such as S_3 of the (001) surface is very small as these states are strongly localized close to the nuclei.]

In Fig. 3 we plot the energy shift of two surface states, S_1 of the majority spin and S_2 of the minority spin, at $\bar{\Gamma}$ for the Ni(111) surface. It is seen that both states shift downward almost linearly with increasing field strength, reflecting the potential lowering in the vacuum region. The downward shift of S_1 implies that the Fermi surface associated with the parabolic S_1 band increases with increasing applied field, which contributes to boosting tunneling current from S_1. At the same time, the lowering of the energy of S_1 leads to a higher surface barrier for electrons from $\bar{\Gamma}$. The additional states becoming occupied in the S_1 band at larger values of $k_\parallel$ will also feel a higher barrier as part of the kinetic energy is used for the movement parallel to the surface. Hence the tunneling current from S_1 is suppressed. The resultant field-emission current from S_1 is determined as a result of the competition between these two factors. The electric field leads to an energetic lowering of S_2, resulting in these states to cross the Fermi level. As a result S_2 begins to contribute to the emission current. As in the case of S_1, the tunneling current from S_2 is also dependent on the competition between the above-mentioned two factors.

The applied field also induces changes in the bulk-state wave functions at the surface. Figure 4 shows the $\mathbf{k}_\parallel$-resolved DOS of the p_z component calculated in a top-layer Ni MT sphere of the Ni(001) surface at $\bar{\Gamma}$. The p_z component of the DOS is expected to give a large contribution to the tunneling current as these states extend significantly into the vacuum. A small peak around −1 eV (marked by an arrow) can be seen for the minority spin even in the absence of an electric field. This peak is attributed to the presence of flat band dispersion for the Λ_1 branch in the bulk caused by the p-d hybridization. The peak is due to a large amplitude of the state at the surface region and it can be enhanced by the applied field. Such a resonace state can be formed as a superposition of the incident and reflected waves for several different k_z values in the narrow energy range of the flat dispersion mentioned above. The peak around −1 eV gives effects on the spin-polarization of the field emission for the Ni(001) surface as discussed in the next section. Although the majority-spin channel also has the corresponding DOS peak at around −1.5 eV, it has negligiblly small contribution to the field emission of the majority-spin Ni(001) electrons because of its deeper energy level.

C. Field emission from Ni surfaces

We start this section with the discussion of the field emission from the Ni(001) surface. Figure 5 shows the calculated tunneling conductance $\Gamma(\epsilon)$ of Ni(001) for $F=0.65$ V/Å. We plot Eqs. (1) and (3) both, which are practically identical because Ni(001) has no occupied surface states near E_F around $\bar{\Gamma}$ in the SBZ. For the majority spin, the s and p_z orbital components hybridized in the Ni 3d bulk bands make a dominant contribution to $\Gamma(\epsilon)$. As the majority-spin d bands are mostly more than 0.5 eV below E_F, their contribution to $\Gamma(\epsilon)$ is very small. As a result, $\Gamma(\epsilon)$ exhibits an exponential decay with decreasing energy as in the case of jellium surfaces. A small shoulder at −0.35 eV coincides with the resonance energy of S_4 near $\bar{\Gamma}$. $\Gamma(\epsilon)$ of the minority spin decays slower than that of the majority spin, which

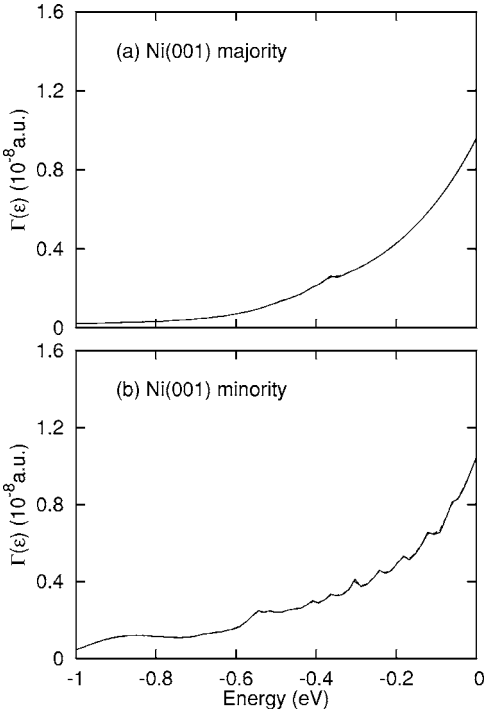

FIG. 5. Field-induced tunneling conductance $\Gamma(\epsilon)$ of Ni(001) for $F=0.65$ V/Å. (a) Majority-spin and (b) minority-spin.

makes the total spin polarization of the field emission from Ni(001) negative. Besides the slower decay of the minority spin $\Gamma(\epsilon)$ one also notes much more structure in its energy dependence and a shallow maximum at around −0.9 eV. These features of $\Gamma(\epsilon)$ are due to the Ni $3d$ surface resonances, mainly S_4, that cross E_F near $\bar{\Gamma}$ as shown in Fig. 1(b). Our analysis has revealed that the $d_{xz,yz}$-orbital components of S_4 contribute to the tunneling current through the hybridization with the p_z-orbital component off $\bar{\Gamma}$. The shallow maximum at around −0.9 eV reflects the peak in the p_z component of the DOS shown in Fig. 4.[49] In Fig. 6 we show

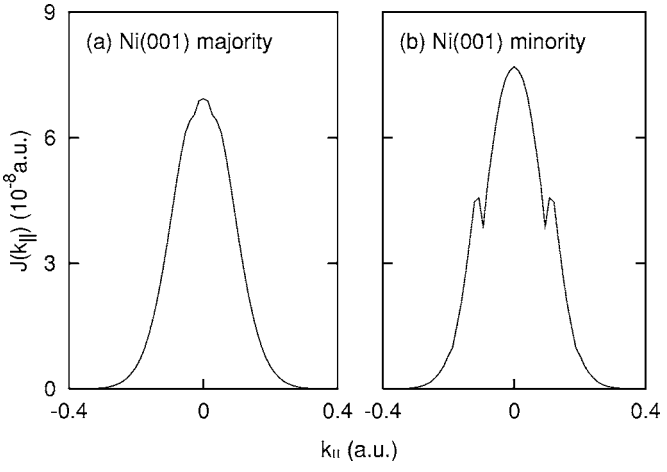

FIG. 6. $J(\mathbf{k}_\parallel)$, $\mathbf{k}_\parallel$-resolved current density, for Ni(001) in the $\bar{\Gamma}$-$\bar{M}$ direction in the SBZ. (a) Majority-spin and (b) minority-spin. $F=0.65$ V/Å. $|\mathbf{k}_\parallel|$ at $\bar{M}$ is 0.95 a.u.

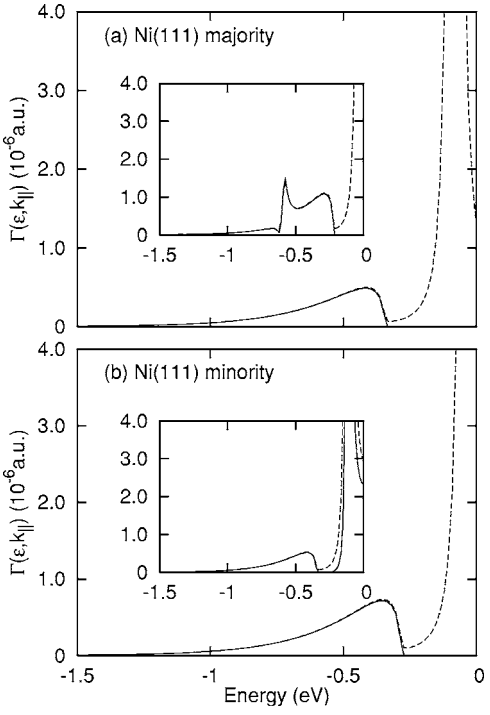

FIG. 7. $\mathbf{k}_\parallel$-resolved tunneling conductance $\Gamma(\epsilon,\mathbf{k}_\parallel)$ of the Ni(111) surface at $\bar{\Gamma}$ for (a) majority spin and (b) minority spin. $F=0.65$ V/Å. Solid and dashed lines express the bulk and total conductance calculated using Eqs. (1) and (3), respectively. The insets show $\Gamma(\epsilon,\mathbf{k}_\parallel)$ slightly off $\bar{\Gamma}$ toward $\bar{M}$, where $|\mathbf{k}_\parallel|=0.02$ a.u. The broadening parameter η in Eq. (4) was chosen as 10^{-4} a.u.

$J(\mathbf{k}_\parallel)$, the $\mathbf{k}_\parallel$ distribution of the emission current, of Ni(001) for $F=0.65$ V/Å. As in the case of jellium and noble-metal surfaces, $J(\mathbf{k}_\parallel)$ for the majority spin exhibits a large single peak centered at $\bar{\Gamma}$, which confirms that the emission current stems mostly from the sp components in the valence bands. $J(\mathbf{k}_\parallel)$ of the minority spin component has an additional narrow peak at a finite $\mathbf{k}_\parallel$, which corresponds to the wave vector where S_4 crosses E_F as one sees in Fig. 1(b).

The field emission from Ni(111) is more complicated than that from Ni(001) because of partially occupied surface states and resonances near $\bar{\Gamma}$ in the SBZ. To demonstrate this, we plot in Fig. 7 the $\mathbf{k}_\parallel$-resolved tunneling conductance $\Gamma(\epsilon,\mathbf{k}_\parallel)$ at $\bar{\Gamma}$, where $F=0.65$ (V/Å). Solid lines show results calculated using the Landauer formula. It is seen that only the bulk Ni band with Λ_1 symmetry containing s, $p_{z'}$, and $d_{3z'^2-r^2}$ components (one of three t_{2g} components at L in the bulk BZ) makes significant contributions to $\Gamma(\epsilon,\mathbf{k}_\parallel)$. In contrast to the majority spin, for the minority spin E_F is located inside the projection of the doubly degenerate Ni Λ_3 bands (e_g component). However, these bands make negligibly small contributions to $\Gamma(\epsilon,\mathbf{k}_\parallel)$. This can be understood as e_g-symmetry orbitals at $\bar{\Gamma}$ are almost lying in the (111) surface of an fcc solid, and have a small weight in the vacuum region.

The dashed lines in Fig. 7 show the total tunneling conductance calculated using Eq. (3). The large peak in the energy gap of the majority spin, which is missing in the solid

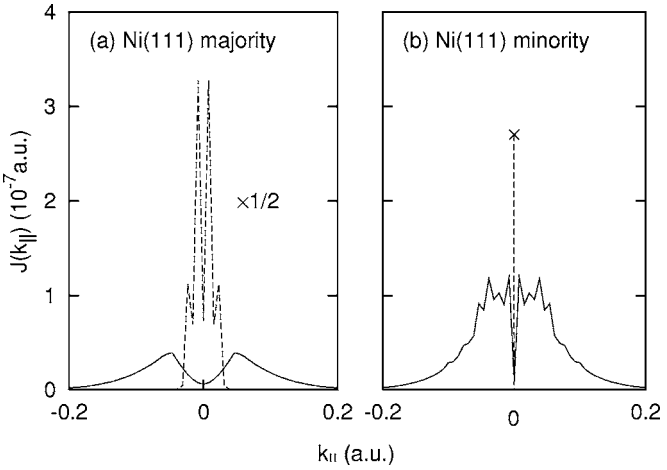

FIG. 8. $J(\mathbf{k}_\parallel)$, $\mathbf{k}_\parallel$-resolved current density, for Ni(111) in the $\bar{\Gamma}$-$\bar{M}$ direction in the SBZ. (a) Majority spin and (b) minority spin. Solid and dashed lines show the bulk-state and surface-state current densities, respectively. $F=0.65$ V/Å. $|\mathbf{k}_\parallel|$ at $\bar{M}$ is 0.67 a.u.

line, corresponds to the surface state S_1 whose energy is about −0.1 eV for $F=0.65$ V/Å (Fig. 3). It is to be noted that while its peak width has no physical meaning, its integrated area remains constant to a high accuracy irrespective of the choice of the broadening parameter η. Similarly, the large peak in Fig. 7(b) originates from S_2 whose energy is about −0.05 eV (Fig. 3). The Landauer formula fails to reproduce this peak, since S_2 is a localized state at $\bar{\Gamma}$. This situation changes rapidly when one moves away from $\bar{\Gamma}$. The insets in Fig. 7 show $\Gamma(\epsilon,\mathbf{k}_\parallel)$ calculated slightly off $\bar{\Gamma}$. S_1 of the majority spin remains a surface state and hence leads to no coherent current as given by the Landauer formula. On the other hand, S_2 of the minority spin turns into a resonance except for $\bar{\Gamma}$ due to symmetry lowering. As a result, the S_2 peak appears in both solid and dashed lines. In this case the width of the peak is determined by the coupling among different Ni 3*d* bands and is physically meaningful.

The above-mentioned variation of $\Gamma(\epsilon,\mathbf{k}_\parallel)$ with energy and $\mathbf{k}_\parallel$ is summarized in Figs. 8 and 9. In Fig. 8 we show $J(\mathbf{k}_\parallel)$ of the Ni(111) surface for $F=0.65$ V/Å. Solid and dashed lines represent the bulk-state and surface-state currents evaluated with Eqs. (1) and (2), respectively. As for the majority spin, the surface-state peak centered at $\bar{\Gamma}$ originates from S_1. Its distribution is limited within the two-dimenisonal Fermi surface of S_1. In the same $\mathbf{k}_\parallel$ range one observes a dip in the bulk-state current, which occurs because E_F is located in the energy gap of the projected Ni bulk bands. As for the minority spin, the surface-state current is limited to $\bar{\Gamma}$, while the bulk-state current nearly vanishes at $\bar{\Gamma}$. The bulk-state current for nonzero $\mathbf{k}_\parallel$ consists of the emission from the surface resonance S_2 as well as that from the bulk states.

Figure 9 shows the tunneling conductance $\Gamma(\epsilon)$ of Ni(111) for $F=0.65$ V/Å. For the majority-spin, the bulk-state conductance (solid line) decays smoothly with decreasing energy as in the case of jellium surfaces. The total conductance

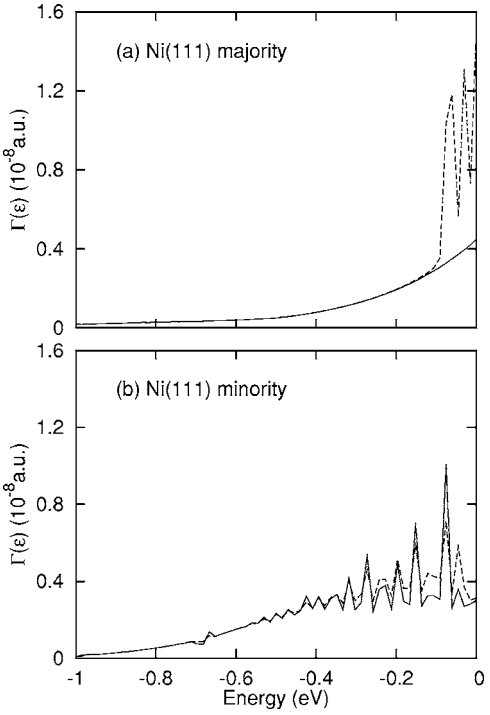

FIG. 9. Field-induced tunneling conductance $\Gamma(\epsilon)$ of Ni(111) for $F=0.65$ V/Å. (a) Majority spin and (b) minority spin.

(dashed line) possesses an additional component due to S_1 whose energy range is limited between E_F and the bottom of the S_1 band ($\approx$−0.1 eV). On the other hand, the minority-spin conductance is a superposition of the exponentially decaying bulk-state contribution and the much larger contribution from the surface resonance S_2. The spiky structure is an artifact that arises because the width of S_2 is very narrow while the $\mathbf{k}_\parallel$ space summation is performed over discrete mesh points. We have systematically increased the number of $\mathbf{k}_\parallel$ points and checked that the present mesh is fine enough to evaluate the current density J. The singular behavior of $J(\mathbf{k}_\parallel)$ at $\mathbf{k}_\parallel=0$ does not lead to a signficant contribution to the total current J because of its negligible weight in the radial integration in the $\mathbf{k}_\parallel$ space.

D. Spin polarization in field-emission current

The spin polarization P is defined as

$$P=\frac{J_\uparrow-J_\downarrow}{J_\uparrow+J_\downarrow}, \tag{7}$$

where $J_{\uparrow(\downarrow)}$ denotes the emitted current density for majority (minority) spin electrons. In Fig. 10, we present the variation of P with the field strength F for the Ni(001) and Ni(111) surfaces. The minus sign indicates that the emitted current is polarized opposite to the magnetization direction.

The calculated $|P|$ for Ni(001) ranges from 7% to 10% for a typical F in field-emission experiments (0.3–0.5 V/Å). The increase in $|P|$ with increasing F values can be partly attributed to the enhancement of the p_z component of the minority-spin DOS (see Fig. 4).

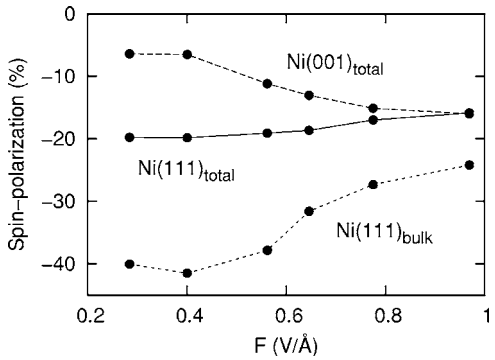

FIG. 10. Spin polarization of the field-emission current for Ni surfaces. Solid line, Ni(111) with both bulk-state and surface-state contributions; dotted line, Ni(111) with only bulk-state contribution; and dashed line, Ni(001).

For Ni(111), the maximum $|P|$ exceeds 40% if one considers only the emission from bulk states (dotted line). This large value originates from the large minority-spin emission from the surface resonance S_2. The emission current from S_2 increases with increasing F, until the S_2 band is completely filled at $F \sim 0.4$ V/Å as seen from Fig. 3. For larger field values, the tunneling current from the resonance diminishes again due to the continued shift toward lower energies, leading to a larger potential barrier for tunneling. The spin polarization of the emitted current from Ni(111) is halved when one adds the majority-spin emission from the surface state S_1 (solid line). It is seen that the total polarization varies only modestly as a function of F. The contribution of S_1 of the majority spin to the field emission decreases for relatively large electric field. Such a behavior can be observed from the difference between the solid and dotted lines in Fig. 10.

The main origin for the negative polarization P can be attributed to the relative position of the d bands in the majority and minority spin states. For the majority spin state the d bands are located more than 0.5 eV below the Fermi level. Hence their contributions (mostly through surface states and surface resonances) to the field-emission current are negligible. The field emission from the majority spin states of Ni is essentially the same as that of noble metals. On the other hand, the minority-spin d bands are located around the Fermi level and they can make appreciable contributions to the field-emission current. The additional contribution coming from the p_z component of the DOS (Fig. 4) can also be assigned to the d state origin because the peak is due to the p-d hybridization.

Experimentally, the spin polarization of field emission from Ni surfaces was measured in the 1970s.[19,20] Our calculated polarization P is in fair agreement with the experimented value, we reproduce the correct sign and the correct trend in the polarization, which was measured to be $-3 \pm 1\%$ for Ni (001). For Ni(111), the measured polarization, $P = -6 \pm 1\%$, is smaller than P in the present calculation but still showing the same sign and tendency. A possible origin of this disagreement may be the electron-correlation effects beyond the LSDA. According to the GW calculation of Aryasetiawan,[50] the energy position of $L_{2'}$ at L of the Ni band structure is by about 0.6 eV lower than that obtained with the LSDA. Some difficulties in experimental studies may also be possible causes of the discrepancy. Although experiments were performed very carefully to achieve a clean and flat surface, it is not totally possible to avoid hydrogen adsorption and the presence of steps, for example. It is known that the hydrogen adsorption reduces the surface magnetic moment and the surface steps reduce the local work function, leading to some ambiguity in the experimental P.

IV. SUMMARY

We have presented results of a first-principles calculation of the spin-polarized field-emission from ferromagnetic Ni(111) and Ni(001) surfaces. The self-consistent electronic structure of both surfaces subject to an applied electric field was calculated using the surface-embedded Green function approach and the FLAPW method within LSDA. We used the conductance formula in Ref. 32 that incorporates tunneling currents from both bulk and surface states.

For the majority-spin channel of Ni(001), surface states and resonances make little contribution to the emitted current, partly because they do not exist close to E_F near $\bar{\Gamma}$ in the SBZ. On the other hand, the emitted current from the minority-spin channel reflects resonance states containing d states contribution to exceed the emitted current of the majority-spin channel. In the case of Ni(111), surface states and surface resonances play a dominant role in the field emission for both spin channels. The partially filled surface band in the energy gap of the projected bulk Ni bands, S_1, makes a large contribution to the majority-spin current, while the surface resonance S_2 contributes more significantly to the minority-spin current.

We have evaluated the spin polarization P of field-emission currents as a function of field strength F. While we can reproduce the experimental findings as far as the sign of the polarization and the trend is concerned when going from Ni(001) to Ni(111), some quantitative details remain to be clarified. This opens the perspective to improve both the experimental characterization of the surfaces and its theoretical description to investigate the influence of these surface details on the tunneling process which would lead to a valuable increase in the understanding the spin-dependent electronic properties of nanostructures on surfaces, such as deposited clusters, stepped surfaces, or wires and chains.

ACKNOWLEDGMENT

This work was partly supported by the NAREGI Nanoscience Project; Ministry of Education, Culture, Sports, Science and Technology, Japan.

APPENDIX

Magaud *et al.*[40] showed the orbital character of the Ni(111)-surface electronic structure obtained with slab calculations, which is in agreement with our results. In Table I, we indicate the orbital character of surface-induced electronic states of the Ni(111) and (001), S_{1-4} shown in Figs. 1 and 2

TABLE I. Characteristics of each surface state and surface resonance of Ni(111) and (001) surfaces.

Surface		Spin	$\mathbf{k}_{\parallel}$	Character[a]	State[b]	Contribution to emission current
(111)	S_1	majority	$\bar{\Gamma}$:	$p_{z'}(+d_{3z'^2-r^2})$	SS	Significant[c]
			off $\bar{\Gamma}$:	mixing of $d_{x'z',y'z'}$	SS	Significant[c]
		minority	$\bar{\Gamma}$:	no weight		None
			off $\bar{\Gamma}$:	$d_{x'z',y'z'}(+p_{z'})$	RS	None
	S_2	majority	$\bar{\Gamma}$:	no weight		None
			off $\bar{\Gamma}$:	$d_{x'z',y'z'}(+p_{z'})$	RS	Negligible
		minority	$\bar{\Gamma}$:	$p_{z'}(+d_{3z'^2-r^2})$	SS	Significant
			off $\bar{\Gamma}$:	mixing of $d_{x'z',y'z'}$	RS	Significant
(001)	S_3	majority	$\bar{\Gamma}$:	$d_{xz,yz}(+p_{x,y})$	RS	None
			$\bar{M}$:	$d_{x^2-y^2}$	SS	None
		minority	$\bar{\Gamma}$:	$d_{xz,yz}(+p_{x,y})$	RS	None
			$\bar{M}$:	$d_{x^2-y^2}$	SS	None
	S_4	majority	$\bar{\Gamma}$:	no weight		None
			off $\bar{\Gamma}$:	$d_{xz,yz}(+p_z)$	RS	Appreciable[d]
		minority	$\bar{\Gamma}$:	no weight		None
			off $\bar{\Gamma}$:	$d_{xz,yz}(+p_z)$	RS	Significant[e]

[a]Parentheses: relatively small mixing with the main component.
[b]SS: surface state, RS: resonance state.
[c]See dashed lines in Figs. 8(a) and 9(a).
[d]See small shoulder in Fig. 5(b).
[e]See narrow peaks in Fig. 6(b).

including information about their contribution to the field-emission current.

We see from Table I that at $\bar{\Gamma}$, the characters of S_1 and S_2 are exchanged between majority and minority spins. It is caused by the fact that two spin channels of Ni crystal have different energy-level ordering for $L_{2'}$ and L_3 at L of the bulk band. In the case of the majority spin, the energy level of $L_{2'}$ is higher than that of L_3, and *vice versa* in the minority spin. According to the irreducible representation for the fcc lattice, $L_{2'}$ has the $p_x+p_y+p_z$ basis in terms of cubic harmonic functions, which turns to the $p_{z'}$ component. The $d_{3z^2-r^2}$ component can hybridize with the $p_{z'}$ on (111) faces of fcc solids. The $L_{2'}$ state having a wave function extending toward the vacuum leads to formation of the surface state: S_1 of the majority spin and S_2 of the minority spin. On the other hand, L_3 corresponds to doubly degenerate e_g states, whose orbitals are more or less confined within (111) faces and do not produce surface states or resonances. These arguments explain the fact that S_1 (S_2) of the majority spin and S_2 (S_1) of the minority spin have (no) weight at $\bar{\Gamma}$.

[1] S. Parkin, C. Kaiser, A. Panchula, P. Rice, B. Hughes, M. Samant, and S.-H. Yang, Nat. Mater. **3**, 862 (2004).
[2] S. Yuasa, T. Nagahama, A. Fukushima, Y. Suzuki, and K. Ando, Nat. Mater. **3**, 868 (2004).
[3] S. Heinze, M. Bode, A. Kubetzka, O. Pietzsch, X. Nie, S. Blügel, and R. Wiesendanger, Science **288**, 1805 (2000).
[4] M. Julliere, Phys. Lett. **54A**, 225 (1975).
[5] D. Wortmann, S. Heinze, Ph. Kurz, G. Bihlmayer, and S. Blügel, Phys. Rev. Lett. **86**, 4132 (2001).
[6] A. Modinos, *Field, Thermionic, and Scondary Electron Emission Scectroscopy* (Plenum Press, New York, 1984).
[7] For a review, see, J. W. Gadzuk and E. W. Plummer, Rev. Mod. Phys. **45**, 487 (1973).
[8] A. Modinos and N. Nicolaou, Phys. Rev. B **13**, 1536 (1976).
[9] A. Modinos, J. Phys. C **9**, 3867 (1976).
[10] P. Soven, E. W. Plummer, and N. Kar, CRC Crit. Rev. Solid State Sci. **1**, 111 (1976).
[11] Y. Gohda, Y. Nakamura, K. Watanabe, and S. Watanabe, Phys. Rev. Lett. **85**, 1750 (2000).
[12] Y. Gohda and S. Watanabe, Phys. Rev. Lett. **87**, 177601 (2001).
[13] Y. Gohda, Y. Nakamura, K. Watanabe, and S. Watanabe, Mater. Sci. Eng., A **327**, 1 (2002).
[14] N. Kobayashi, K. Hirose, and M. Tsukada, Appl. Surf. Sci. **237**, 572 (2004).
[15] T. Ohwaki, H. Ishida, and A. Liebsch, Phys. Rev. B **68**, 155422 (2003).
[16] I. Merrick, J. E. Inglesfield, and G. A. Attard, Phys. Rev. B **72**, 033403 (2005).

[17] W. Gleich, G. Regenfus, and R. Sizmann, Phys. Rev. Lett. **27**, 1066 (1971).
[18] N. Müller, Phys. Lett. **54A**, 415 (1975).
[19] M. Landolt and M. Campagna, Phys. Rev. Lett. **38**, 663 (1977).
[20] M. Campagna, S. F. Alvarado, and E. Kisker, *Polarized Electrons from Metallic System*, in *Electrons in Disordered Metals and at Metallic Surfaces* (Plenum Press, New York, 1979).
[21] B. A. Politzer and P. H. Cultler, Phys. Rev. Lett. **28**, 1330 (1972).
[22] J.-N. Chazalviel and Y. Yafet, Phys. Rev. B **15**, 1062 (1977).
[23] A. Modinos and G. Oxinos, Inst. Phys. Conf. Ser. **55**, 157 (1981).
[24] J. Zavadil and A. Modinos, J. Phys. C **15**, 7255 (1982).
[25] J. Inglesfield, J. Phys. C **14**, 3795 (1981).
[26] H. Ishida, Phys. Rev. B **63**, 165409 (2001).
[27] D. Wortmann, H. Ishida, and S. Blügel, Phys. Rev. B **65**, 165103 (2002).
[28] The differences in the work function and the surface magnetic moment between two- and three-atomic-layer calculations for Ni(111), for example, are only 0.02 eV and $0.01\mu_B$, respectively. It indicates that the two atomic layers are sufficient as the embedded surface region.
[29] In Sec. III, we discuss the surface electronic structures of Ni surfaces in terms of orbital components of Ni bands, and it must be noted that the index for the orbital is defined differently for each surface. As for the relationship for the *d*-orbital indices between the (001) and (111) faces, see, for example, K. Terakura, T. Oguchi, A. R. Williams, and J. Kübler, Phys. Rev. B **30**, 4734 (1984).
[30] R. Landauer, Philos. Mag. **21**, 863 (1970).
[31] M. Büttiker, Phys. Rev. Lett. **57**, 1761 (1986).
[32] H. Ishida, D. Wortmann, and T. Ohwaki, Phys. Rev. B **70**, 085409 (2004).
[33] D. Wortmann, H. Ishida, and S. Blügel, Phys. Rev. B **66**, 075113 (2002).
[34] C. S. Wang and A. J. Freeman, Phys. Rev. B **21**, 4585 (1980).
[35] E. Wimmer, A. J. Freeman, and H. Krakauer, Phys. Rev. B **30**, 3113 (1984).
[36] C. L. Fu and A. J. Freeman, J. Phys. C **8**, 1625 (1988).
[37] M. Aldén, S. Mirbt, H. L. Skriver, N. M. Rosengaard, and B. Johansson, Phys. Rev. B **46**, 6303 (1992).
[38] A. A. Ostroukhov, V. M. Floka, and V. T. Cherepin, Surf. Sci. **331-333**, 1388 (1995).
[39] F. Mittendorfer, A. Eichler, and J. Hafner, Surf. Sci. **423**, 1 (1999).
[40] L. Magaud, A. Pasturel, P. Mallet, S. Pons, and J. Y. Veuillen, Europhys. Lett. **67**, 90 (2003).
[41] M. I. Haftel, N. Bernstein, M. J. Mehl, and D. A. Papaconstantopoulos, Phys. Rev. B **70**, 125419 (2004).
[42] H. C. Lu, E. P. Gusev, E. Garfunkel, and T. Gustafsson, Surf. Sci. **352-354**, 21 (1996).
[43] J. M. W. Frenken, R. G. Smeenk, and J. F. Van der Veen, Surf. Sci. **135**, 147 (1983).
[44] H. B. Michaelson, J. Appl. Phys. **48**, 4729 (1977).
[45] Note that S_3 exists as a resonance state in the whole range between $\bar{\Gamma}$ and M, though some part of S_3 is invisible in Fig. 1. This is just due to the fact that the height of the corresponding DOS peak is relatively low as compared with the DOS peaks of other surface-induced states.
[46] The value, 0.005 eV, however, is near the accuracy limit of our calculation and even the sign may change depending on the computational conditions. Nevertheless, the energy position of S_1 deepens significantly under external electric field as shown in Fig. 3.
[47] M. Donath, F. Passek, and V. Dose, Phys. Rev. Lett. **70**, 2802 (1993).
[48] F. Passek and M. Donath, Phys. Rev. Lett. **71**, 2122 (1993).
[49] The DOS peak of the p_z component shown in Fig. 4 is seen at around −1 eV, which deviates from the position of the shallow maximum of $\Gamma(\epsilon)$ at around −0.9 eV shown in Fig. 5(b). This deviation is caused by the energy shift of the corresponding DOS peak off $\bar{\Gamma}$.
[50] F. Aryasetiawan, Phys. Rev. B **46**, 13051 (1992).